Journal Pre-proof

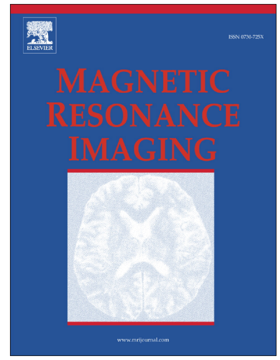

Optimization of a transmit/receive surface coil for squirrel monkey spinal cord imaging

Ming Lu, Feng Wang, Li Min Chen, John C. Gore, Xinqiang Yan

PII: S0730-725X(20)30039-4

DOI: https://doi.org/10.1016/j.mri.2020.02.011

Reference: MRI 9389

To appear in: *Magnetic Resonance Imaging*

Received date: 25 January 2020

Revised date: 14 February 2020

Accepted date: 15 February 2020

Please cite this article as: M. Lu, F. Wang, L.M. Chen, et al., Optimization of a transmit/receive surface coil for squirrel monkey spinal cord imaging, *Magnetic Resonance Imaging*(2020), https://doi.org/10.1016/j.mri.2020.02.011

Technical Note

Optimization of a transmit/receive surface coil for squirrel monkey spinal cord imaging

Ming Lu[1,2,3], Feng Wang[1,2], Li Min Chen[1,2], John C. Gore[1,2,4,5,6], Xinqiang Yan[1,2]

[1]Vanderbilt University Institute of Imaging Science, Vanderbilt University Medical Center, Nashville, Tennessee, USA

[2]Department of Radiology and Radiological Sciences, Vanderbilt University Medical Center, Nashville, Tennessee, USA

[3]College of Nuclear Equipment and Nuclear Engineering, Yantai University, Yantai, Shandong, China

[4]Department of Biomedical Engineering, Vanderbilt University, Nashville, Tennessee, USA

[5]Department of Physics and Astronomy, Vanderbilt University, Nashville, Tennessee, USA

[6] Department of Molecular Physiology and Biophysics, Vanderbilt University, Nashville, Tennessee, USA

Correspondence to Xinqiang Yan: xinqiang.yan@vanderbilt.edu
Vanderbilt University Medical Center
1161 21st Avenue South
Medical Center North, AA-3111
Nashville, TN 37232-2310
Tel: 615-525-3989

Abstract:

MR Imaging the spinal cord of non-human primates (NHP), such as squirrel monkey, is important since the injuries in NHP resemble those that afflict human spinal cords. Our previous studies have reported a multi-parametric MRI protocol, including functional MRI, diffusion tensor imaging, quantitative magnetization transfer and chemical exchange saturation transfer, which allows non-invasive detection and monitoring of injury-associated structural, functional and molecular changes over time. High signal-to-noise ratio (SNR) is critical for obtaining high-resolution images and robust estimates of MRI parameters. In this work, we describe our construction and use of a single channel coil designed to maximize the SNR for imaging the squirrel monkey cervical spinal cord in a 21 cm bore magnet at 9.4T. We first numerically optimized the coil dimension of a single loop coil and then evaluated the benefits of a quadrature design. We then built an optimized coil based on the simulation results and compared its SNR performance with a non-optimized single coil in both phantoms and in vivo.

Keywords: MRI; RF coil; Signal-to-noise ratio; Spinal cord imaging; Non-human primates

Introduction

The normal structures and functions of the spinal cord can be disrupted by traumatic spinal cord injuries (SCI). Controlled injuries to the spines of non-human primates resemble those that afflict human spinal cords, and imaging studies of injury models allow for applying and evaluating multiple advanced quantitative MRI methods to delineate the damage. For example, selective transection of the dorsal column allows for longitudinal studies of injury and recovery across specific spinal segments around the lesioned site [1-6]. Our previous studies have reported a multi-parametric MRI protocol, including functional MRI (fMRI), diffusion tensor imaging (DTI), quantitative magnetization transfer (qMT) and chemical exchange saturation transfer (CEST), which allows non-invasive detection and monitoring of injury-associated structural, functional and molecular changes over time [1-6]. Multi-parametric MRI of small spinal cords relies on the ability to robustly acquire images with different data acquisition parameters. High signal-to-noise ratio (SNR) is critical for obtaining high resolution images and robust estimates of MRI parameters [7]. However, compromises on image quality have to be made by considerations of spatial resolution, data acquisition time and SNR for each imaging session. The squirrel monkey cervical cord is ~4 × 6 mm^2 in cross-section, and an in-plane resolution of better than 0.5 × 0.5 mm^2 is needed to reliably identify white matter and gray matter in the cord. Thus, it is critical to customize a coil which can provide the desired B_1 coverage and high SNR for imaging selected spinal cord segments of interest. Using a customized coil confined to the region of interest also minimizes unwanted signals from moving tissues located farther away.

Radiofrequency (RF) coil design is critical in terms of SNR and B_1 uniformity. A combination of body coil and closely-fitting receive-only array (Tx + Rx) can achieve a uniform transmit field and high sensitivity in reception and such combinations are widely used for clinical scanners. However, such an arrangement requires multiple receivers and a separate transmitting coil and associated detuning circuits that take up precious space and are not always available on smaller bore animal scanners. Surface coils for both transmission and reception are widely used for small field of view (FOV) applications in small animal imaging [8], such as for the spinal cord. A commonly used design is a single L/C loop that resonates at the desired frequency. The loop's dimensions have a major effect on the coil's B_1 efficiency, including determining both the transmit (B_1^+) and receive (B_1^-) fields. In addition to a single coil, a quadrature arrangement consisting of two orthogonal coils is also widely used, especially as partial volume coils [9-13]. These two coils may be two loops or a combination of one loop with another component (such as a microstrip line or figure-of-eight coil). The use of quadrature coils can increase the B_1 efficiency (both B_1^+ and B_1^-) and is compatible with a single channel transmit/receive system by simply adding a hybrid coupler, even though it may have two component coils.

In this work, we describe our construction and use of a single channel coil designed to maximize the SNR for imaging the squirrel monkey cervical spinal cord in a 21 cm bore magnet at 9.4T. We first numerically optimized the coil dimension of a single loop coil and then evaluated the benefits of a quadrature design. We then built an optimized coil based on the simulation results and compared its SNR performance with a non-optimized single coil in both phantoms and in vivo.

Materials and Methods

1. Coil optimization

We first optimized the L/C loop coil size through full-wave electromagnetic (EM) simulation to achieve a maximize SNR at a target area with a depth of approximate 1.5 cm. Since SNR is proportional to the receive field (B_1^-) efficiency, herein we used the B_1^- efficiency as the critique to evaluate coil performance in numerical calculations. The B_1^- efficiency of a single coil was defined by the ratio between B_1^- and the root mean square of the input power [14], where B_1^- maps were extracted from the simulation by the following equation [15]:

$$B_1^- = \frac{\left(B_x - iB_y\right)^*}{2}$$

The length of the rectangular coil was kept to 3 cm to fit the squirrel monkey's neck and cover all segments of their cervical spinal cords. The coil width was varied between 6 cm and 2 cm in 1 cm steps, as shown in Figure 1A. Each coil was mounted on a 4.5-cm-diameter cylindrical surface which approaches the curvature of a squirrel monkey's neck. After obtaining the optimized coil width, we further investigated the SNR improvement from a quadrature surface coil design. For this, two loops of identical size as the optimized single coil were overlapped ~10% to minimize mutual inductive coupling [16].

Numerical optimizations were performed by an FEM-method based solver (HFSS, Ansys Corporation. Canonsburg, PA, USA) [17, 18]. Figures 1C and 1D show the simulation models of a single loop and a quadrature coil respectively. Each coil was tuned to 400.6 MHz and matched to 50 ohm. A 4-cm-diameter cylindrical phantom with similar electromagnetic parameters as animal tissues (conductivity σ=0.4 S/m and relative primitivity ξ_r=74) [19] was used as loading. Coils were placed 3 mm below the phantom. In the simulation, the distance of a radiation boundary and coils was larger than half wavelength, $\lambda/2$. The manual meshes were used to accelerate simulation convergence and the convergence condition ΔS (the difference between each adaptive pass) was set to 0.002 to achieve more reliable results. The single loop coil was excited with 1-Watt power, whereas for the quadrature arrangement each coil was excited with 0.5-Watt power with a 90-degree phase shift between them.

2. Coil fabrication and MR experiment

A quadrature surface coil (width of each loop 3 cm) was constructed based on the EM simulation. The coil housing was designed using mechanical design software (SolidWorks Corp., Santa Monica, CA) and directly printed using a 3D printer (ProJet HD 3500 Plus, 3D Systems, USA), as shown in Figure 2. Tin-coated copper wires of 14-AWG (diameter 1.63 mm, Belden 8012) were used as conductors. Each loop had two variable capacitors for tuning and matching (model 5641, Johanson Manufacturing, NJ), as shown in Figure 2A. For small animal applications, it is generally required to have some remote tune and match adjustments as resonant frequency and/or impedances can be shifted significantly by samples and shielding. A 1-meter-long home-built tuning rod was attached to each trimmer capacitor. One end of the tuning rods extended outside the MR bore so the users can easily tune and match the coil remotely. One distributed capacitor (3.3 pF, 111C series, Passive Plus) was positioned at the opposite position of the feed port to segment the conductor and avoid antenna effects. Float baluns were used for each cable to minimize the common-mode current at the high frequency. The overlapped area between the two loops was carefully adjusted to minimize the mutual inductance. As a comparison, we also built a non-optimized comparison single loop with a width of 6 cm.

Both the optimized quadrature 3-cm-wide coil and the non-optimized 6-cm-wide coil were tested in a 9.4 T Varian small animal scanner with 12-cm-diameter clear bore within the gradients. MR images were acquired of a 4-cm-diameter saline phantom (2.0 g/L NaCl and 1.25 g/L $CuSO_4 \times 5H_2O$). The RF power to achieve a 90-degree pulse was calibrated for each coil on a coronal plane 1.5 cm away from the bottom. Low flip angle gradient recalled echo (GRE) images with the following parameters were acquired for SNR calculations on the phantom: FOV = 45 × 45 mm^2, TR/TE = 1000/4 ms, Flip angle = 20 degree, Matrix = 192 × 192, Bandwidth = 260.4 Hz/pixel, Slice thickness = 2 mm and Number of acquisitions = 1.

We also acquired in vivo structural GRE images on a squirrel monkey using the following parameters: FOV = 40 × 40 mm^2, TR/TE = 220/2.874 ms, Flip angle = 40 degree, Matrix = 128 × 128, Bandwidth = 390.6 Hz/pixel, slice thickness = 2/0.75/0.5 mm for axial/sagittal/coronal slices, and number of acquisitions = 4/8/12 for axial/sagittal/coronal slices. For in vivo MR experiments, all procedures followed NIH guidelines on the care and use of laboratory animals. SNR values were calculated as *SI*/*std*(noise), where *SI* is the signal and *std*(noise) is the standard deviation of the noise.

<u>Results</u>

1. Simulated Performance

Figures 3A shows simulated axial B_1^- efficiency (proportional to SNR) maps in the central slice. Average B_1^- efficiency in a 1.5-cm-deep circle area (5mm diameter) are marked in red color. The position and dimension of the circle area are chosen to match the depth and geometry of cervical spinal cords in squirrel monkeys. Figure 3B shows B_1^- efficiency 1D profiles as white dotted lines of Figure 3A.

Smaller coils exhibit higher B_1^- efficiency at the surface, and lower B_1^- efficiency in deeper regions. Therefore, there exists an optimal coil size for any desired depth. At 1.5-cm-deep, the 6-cm-wide loop coil exhibits lower B_1^- efficiency as it is too large and couples to noise from unwanted areas. The B_1^- efficiency increases as the coil width decreases from 6 cm to 3 cm. When the coil width was reduced to 2 cm, however, B_1^- efficiency at 1.5-cm depth dropped as expected. The optimal coil width for this application is approximate 3 cm, which exhibits 42% higher efficiency compared to the 6-cm-wide coil (11.80 vs. 8.33 uT/√W). We also found that the output can be further improved by 41% by using a quadrature design (from 11.80 to 16.64 uT/√W).

2. Bench test

Both the non-optimized 6-cm-wide single coil and the optimized 3-cm-wide quadrature coil were tuned to 400.6 MHz and matched to 50 ohm on the bench with scattering parameter S_{11} better than -30 dB, and were finely retuned and/or rematched when positioned in the MR bore by remotely adjusting the trimmers through tuning rods. For the quadrature coil with two coil elements, an inter-element isolation of -16.6 dB was achieved when loaded with the saline water phantom (Figure 2C). We also checked the inter-element isolation with different loading cases such as ex-vivo squirrel monkey brain and spine, and found that it is always better than -15 dB.

3. Measured SNR

Figures 4A and 4B show measured axial SNR maps on the saline phantom with a non-optimized 6-cm-wide single coil and the optimized 3-cm-wide quadrature coil, respectively. Note that different color scales are used due to the huge SNR difference. Compared to the non-optimized coil, the optimized quadrature coil exhibits 3.2 times SNR improvement at the 1.5-cm-deep area (305.2 vs. 95.5). Figure 5 shows in vivo structural images in transverse, sagittal and cornel slices using these coils. It is clear that the image quality is much improved. In vivo axial SNR maps are also shown in Figures 5D and 5H. Similar to measured SNR on phantoms (Figure 4), the optimized quadrature coil exhibits significant SNR improvement in the spinal cord area compared to the non-optimized coil (82.3 vs. 21.1). For this specific subject, the spinal cord is ~1cm deep and thus higher SNR improvement is found (up to 3.9 times).

Discussion

Although there exists a simple design rule for loop coils to achieve best SNR performance at a given depth (for circular coil, coil radius = depth/√5) [20,21], this rule is derived under the following assumptions: (1) the coil is flat, (2) the loading is an infinite and uniformly conducting half-space, and (3) the coil noise is neglectable. For this application, however, the coil is curved to fit the monkey's spinal cord, and the coil noise becomes non-neglectable when the coil size is less than 3 cm. We found that the optimum coil width should be approximate 3 cm to image spinal cord residing 1.5 cm deep in the body based on the full-wave EM simulation.

As can be seen from the simulation (Figure 3) and imaging experiments (Figure 4), a bright spot appears near the overlapping area of the two loops in the quadrature coil. This is caused by the close placement of the two conductors and can be ameliorated by a gapped design with advanced decoupling methods, such as a capacitive/inductive network [22], induced current elimination decoupling [23-25] and self-decoupling [26]. Here the bright spot exists only at the so it does not affect the MR images in the spinal cord >1cm deep.

In this work, the quadrature design with two coils works in transmit/receive mode where we split the transmit RF power to the two coils and combine the received signals with a hybrid coupler. The advantage of this is the simple hardware setup and the lack of a need for multiple receivers and additional hardware. It should be noted that the quadrature coils could work in a receive-only mode with the two coils connected to two separate preamplifiers and independent receivers. However, the receive-only quadrature coils require an additional transmit coil (body coil) and PIN drivers to detune Tx/Rx coils during reception/transmission.

In addition to the two overlapped loops, there are other geometries that can realize quadrature operation, such as the combination of a loop coil with a figure-of-8 coil, a microstrip line coil [13], a dipole antenna [27, 28] or a monopole antenna [29]. Herein we focus only on the comparison between a widely-used quadrature coil with a single-channel receiver for a specific application. We believe the B_1 efficiency improvement found here can also be achieved by other kinds of quadrature coils. However, it should be noted that simple straight dipoles may not be good candidates for this application as their lengths are much longer than the FOV and will contribute noise from unwanted areas.

Conclusion

We numerically optimized, built and evaluated a transmit/receive surface coil for squirrel monkey spinal cord imaging at 9.4 T. Using this design, the SNR can be significantly improved over simpler coils using a quadrature design with only a single receiver channel.

Acknowledgements

This work was supported by NIH grant NS092961 and DOD grant W81XWH-17-1-0304. The authors thank Mr. Gary Drake for fabricating the tuning rods.

References

1. Wang F, Qi HX, Zu Z, Mishra A, Tang C, Gore JC, et al. Multiparametric MRI reveals dynamic changes in molecular signatures of injured spinal cord in monkeys. Magn Reson Med. 2015;74(4):1125-37. Epub 2014/10/22. doi: 10.1002/mrm.25488. PubMed PMID: 25334025; PubMed Central PMCID: PMCPMC4405405.

2. Wang F, Li K, Mishra A, Gochberg D, Chen LM, Gore JC. Longitudinal assessment of spinal cord injuries in nonhuman primates with quantitative magnetization transfer. Magn Reson Med. 2016;75(4):1685-96. doi: 10.1002/mrm.25725. PubMed PMID: WOS:000372910900030.

3. Chen LM, Mishra A, Yang PF, Wang F, Gore JC. Injury alters intrinsic functional connectivity within the primate spinal cord. P Natl Acad Sci USA. 2015;112(19):5991-6. doi: 10.1073/pnas.1424106112. PubMed PMID: WOS:000354390600051.

4. Wang F, Zu ZL, Wu RQ, Wu TL, Gore JC, Chen LM. MRI evaluation of regional and longitudinal changes in Z-spectra of injured spinal cord of monkeys. Magn Reson Med. 2018;79(2):1070-82. doi: 10.1002/mrm.26756. PubMed PMID: WOS:000419134600049.

5. Wu TL, Yang PF, Wang F, Shi ZY, Mishra A, Wu RQ, et al. Intrinsic functional architecture of the non-human primate spinal cord derived from fMRI and electrophysiology. Nat Commun. 2019;10. doi: ARTN 1416

10.1038/s41467-019-09485-3. PubMed PMID: WOS:000462721900015.

6. Yang PF, Wang F, Chen LM. Differential fMRI activation patterns to noxious heat and tactile stimuli in the primate spinal cord. J Neurosci. 2015;35(29):10493-502. doi: 10.1523/Jneurosci.0583-15.2015. PubMed PMID: WOS:000358299500011.

7. Wang F, Wu TL, Li K, Chen LM, Gore JC. Spatiotemporal trajectories of quantitative magnetization transfer measurements in injured spinal cord using simplified acquisitions. Neuroimage Clin. 2019;23:doi: 10.1016/j.nicl.2019.101921. doi: UNSP 101921

10.1016/j.nicl.2019.101921. PubMed PMID: WOS:000485804400119.

8. Doty FD, Entzminger G, Kulkarni J, Pamarthy K, Staab JP. Radio frequency coil technology for small-animal MRI. NMR Biomed. 2007;20(3):304-25. Epub 2007/04/25. doi: 10.1002/nbm.1149. PubMed PMID: 17451180.

9. Hyde JS, Jesmanowicz A, Grist TM, Froncisz W, Kneeland JB. Quadrature detection surface coil. Magn Reson Med. 1987;4(2):179-84. Epub 1987/02/01. doi: 10.1002/mrm.1910040211. PubMed PMID: 3561247.

10. Stensgaard A. Planar quadrature coil design using shielded-loop resonators. J Magn Reson. 1997;125(1):84-91. Epub 1997/03/01. doi: 10.1006/jmre.1996.1103. PubMed PMID: 9245363.

11. Peshkovsky AS, Kennan RP, Fabry ME, Avdievich NI. Open half-volume quadrature transverse electromagnetic coil for high-field magnetic resonance imaging. Magn Reson Med. 2005;53(4):937-43. Epub 2005/03/31. doi: 10.1002/mrm.20422. PubMed PMID: 15799051.

12. Adriany G, Gruetter R. A half-volume coil for efficient proton decoupling in humans at 4 tesla. J Magn Reson. 1997;125(1):178-84. Epub 1997/03/01. doi: 10.1006/jmre.1997.1113. PubMed PMID: 9245377.

13. Kumar A, Bottomley PA. Optimized quadrature surface coil designs. MAGMA. 2008;21(1-2):41-52. Epub 2007/12/07. doi: 10.1007/s10334-007-0090-2. PubMed PMID: 18057975; PubMed Central PMCID: PMCPMC2588669.

14. Edelstein WA, Glover GH, Hardy CJ, Redington RW. The intrinsic signal-to-noise ratio in NMR imaging. Magn Reson Med. 1986;3(4):604-18. Epub 1986/08/01. doi: 10.1002/mrm.1910030413. PubMed PMID: 3747821.

15. Hoult DI. The principle of reciprocity in signal strength calculations—a mathematical guide. 2000;12(4):173-87.

16. Roemer PB, Edelstein WA, Hayes CE, Souza SP, Mueller OMJMrim. The NMR phased array. Magn Reson Med. 1990;16(2):192-225.

17. Kozlov M, Turner R. Fast MRI coil analysis based on 3-D electromagnetic and RF circuit co-simulation. J Magn Reson. 2009;200(1):147-52. Epub 2009/07/03. doi: 10.1016/j.jmr.2009.06.005. PubMed PMID: 19570700.

18. Yan X, Ma C, Shi L, Zhuo Y, Zhou XJ, Wei L, et al. Optimization of an 8-channel loop-array coil for a 7 T MRI system with the guidance of a co-simulation approach. Appl Magn Reson. 2014;45(5):437-49.

19. Doty FD, Entzminger G, Jr., Hauck CD, Staab JP. Practical aspects of birdcage coils. J Magn Reson. 1999;138(1):144-54. Epub 1999/05/18. doi: 10.1006/jmre.1998.1703. PubMed PMID: 10329237.

20. Wang J, Reykowski A, Dickas J. Calculation of the signal-to-noise ratio for simple surface coils and arrays of coils [magnetic resonance imaging]. IEEE Trans Biomed engineering. 1995 Sep;42(9):908-17.

21. Bottomley PA, Olivieri CH, Giaquinto R. What is the optimum phased array coil design for cardiac and torso magnetic resonance?. Magnetic resonance in medicine. 1997 Apr;37(4):591-9.

22. Lee RF, Giaquinto RO, Hardy CJ. Coupling and decoupling theory and its application to the MRI phased array. Magn Reson Med. 2002;48(1):203-13. Epub 2002/07/12. doi: 10.1002/mrm.10186. PubMed PMID: 12111947.

23. Li Y, Xie Z, Pang Y, Vigneron D, Zhang X. ICE decoupling technique for RF coil array designs. Med phys. 2011;38(7):4086-93.

24. Yan X, Gore JC, Grissom WA. New resonator geometries for ICE decoupling of loop arrays. J Magn Reson. 2017;277:59-67.

25. Yan X, Zhang X, Feng B, Ma C, Wei L, Xue R. 7T transmit/receive arrays using ICE decoupling for human head MR imaging. IEEE Trans Med imaging. 2014;33(9):1781-7.

26. Yan X, Gore JC, Grissom WA. Self-decoupled radiofrequency coils for magnetic resonance imaging. Nat Commun. 2018;9(1):3481. Epub 2018/08/30. doi: 10.1038/s41467-018-05585-8. PubMed PMID: 30154408; PubMed Central PMCID: PMCPMC6113296.

27. Wiggins GC, Zhang B, Lattanzi R, Chen G, Sodickson D, editors. The electric dipole array: an attempt to match the ideal current pattern for central SNR at 7 Tesla. Proceedings of the 20th Annual Meeting of ISMRM, Melbourne, Australia; 2012.

28. Raaijmakers A, Ipek O, Klomp DW, Possanzini C, Harvey P, Lagendijk JJ, et al. Design of a radiative surface coil array element at 7 T: the single-side adapted dipole antenna. Magn Reson M18.

29. Yan X, Wei L, Xue R, Zhang X. Hybrid monopole/loop coil array for human head MR imaging at 7T. Appl Magn Reson. 2015;46(5):541-50. Epub 2015/06/30. doi: 10.1007/s00723-015-0656-5. PubMed PMID: 26120252; PubMed Central PMCID: PMCPMC4479412.

Figure 1 A and **B**: Diagrams of a single loop coil and a quadrature coil consisting of two overlapped loops. **C** and **D**: Simulation models of the single coil and the quadrature coil. For the single loop coil, the coil width was varied from 6 cm to 2 cm for SNR optimization. For the quadrature coil, the coil width was set with the optimum value from Figure 1A.

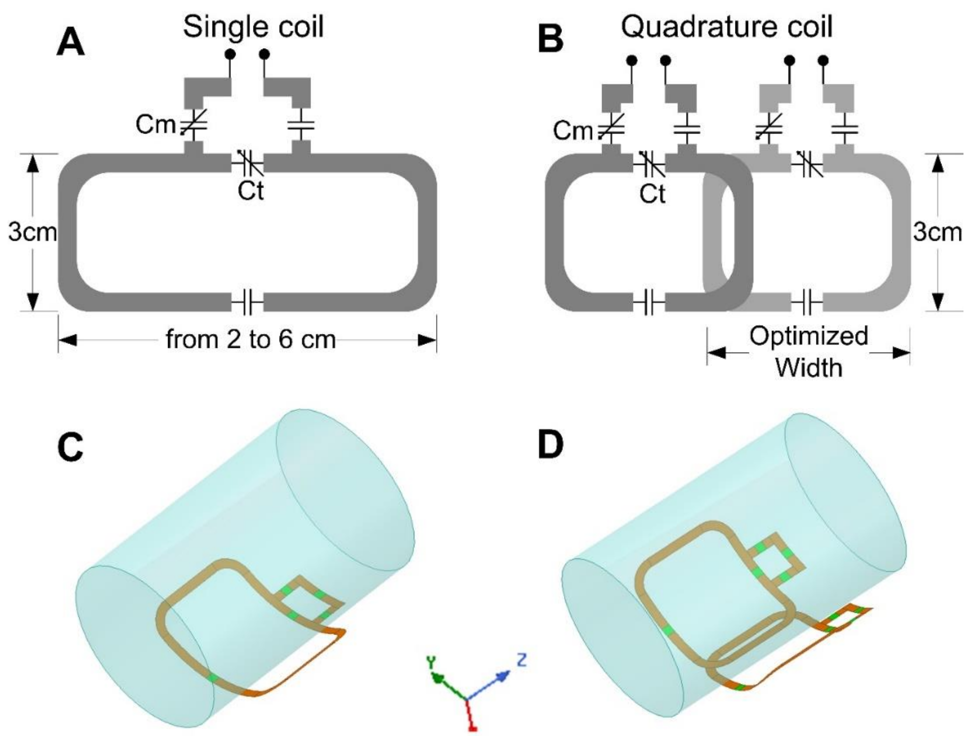

Figure 2 A and **B**: Mechanical drawing and photograph of the quadrature coil with optimized coil width. C: Measured scattering (S-) parameter plots of the quadrature coil when loaded with a 4-cm-diameter phantom (2.0 g/L NaCl and 1.25 g/L $CuSO_4 \times 5H_2O$).

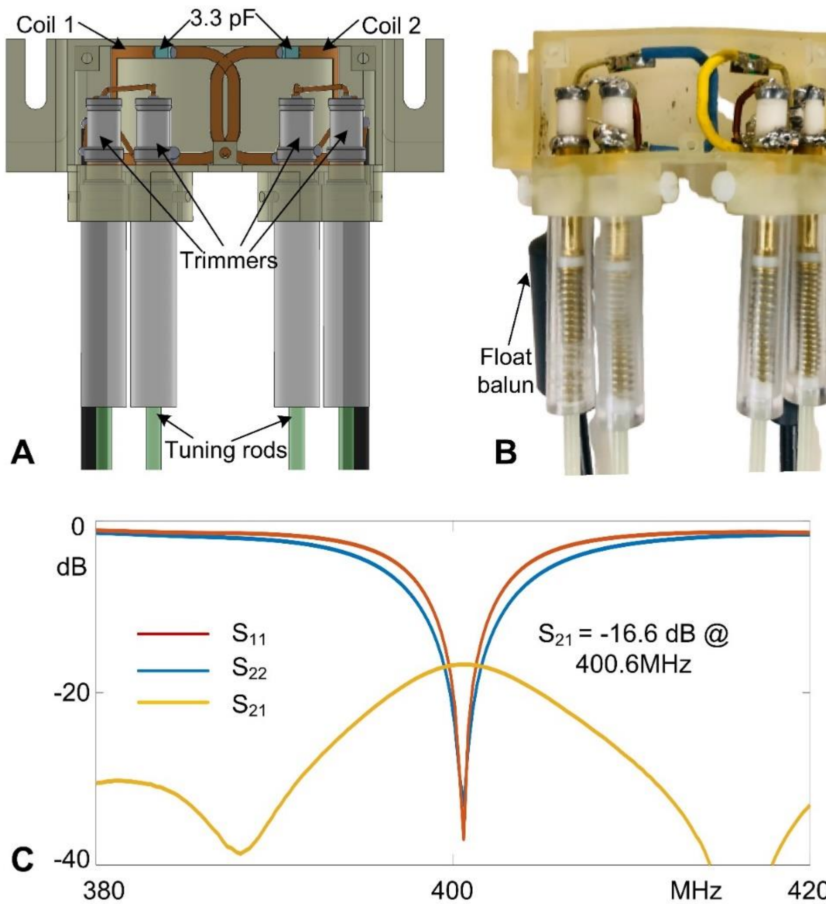

Figure 3 A: Simulated axial maps of B_1^- efficiency ($B_1^-/\sqrt{Power}$) for single coils with various coil widths (from 2 cm to 6 cm) and a quadrature coil with the optimized coil width (3 cm). Average B_1^- efficiencies in the dotted dark circle is marked in each panel. **B**: 1D profiles of the B_1^- efficiency along the dotted white line in Figure 3A. The optimum coil width is 3 cm to maximize the SNR at 1.5-cm depth.

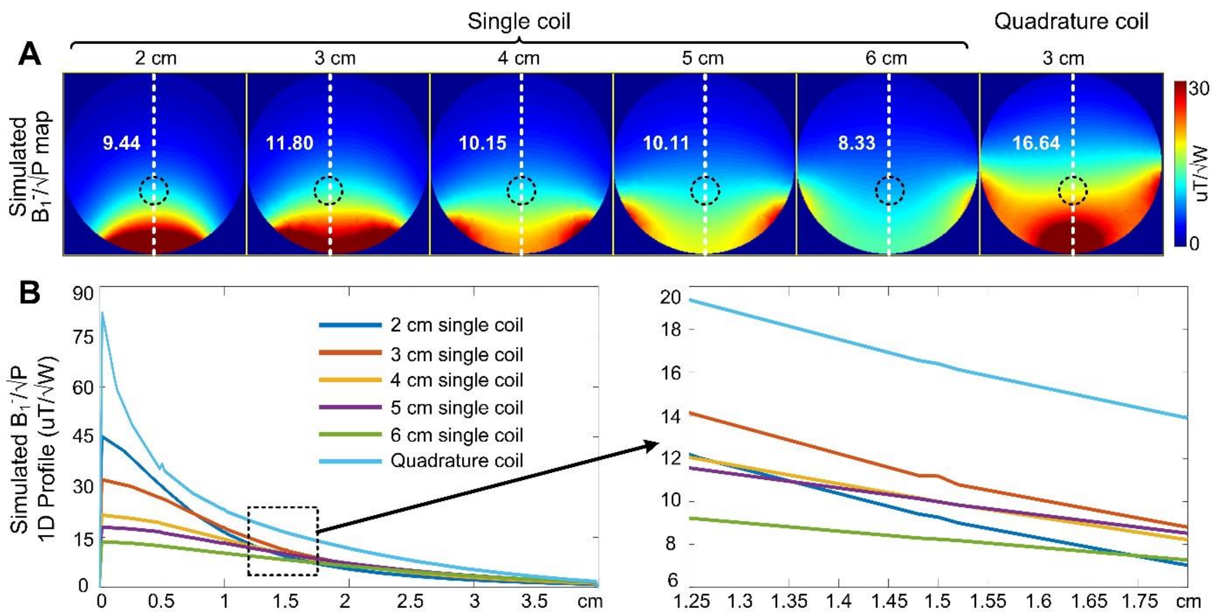

Figure 4 A: Measured SNR on the phantom using non-optimized 6-cm-wide coil and an optimized 3-cm-width quadrature coil. The SNR are calculated from a low-flip-angle GRE images as SNR = *SI*/*std*(noise), where *SI* is the imaging sensitivity and *std*(noise) is the standard deviation of the noise in four corners. Average measured SNRs in the dotted dark circle are marked in each panel. Note that different color scales are used due to the huge SNR difference. **B**: 1D profiles of the measured SNR along the dotted white line in Figure 3A. Compared to the non-optimized coil, the optimized one has 3.2 times SNR improvement at the 1.5-cm-depth area.

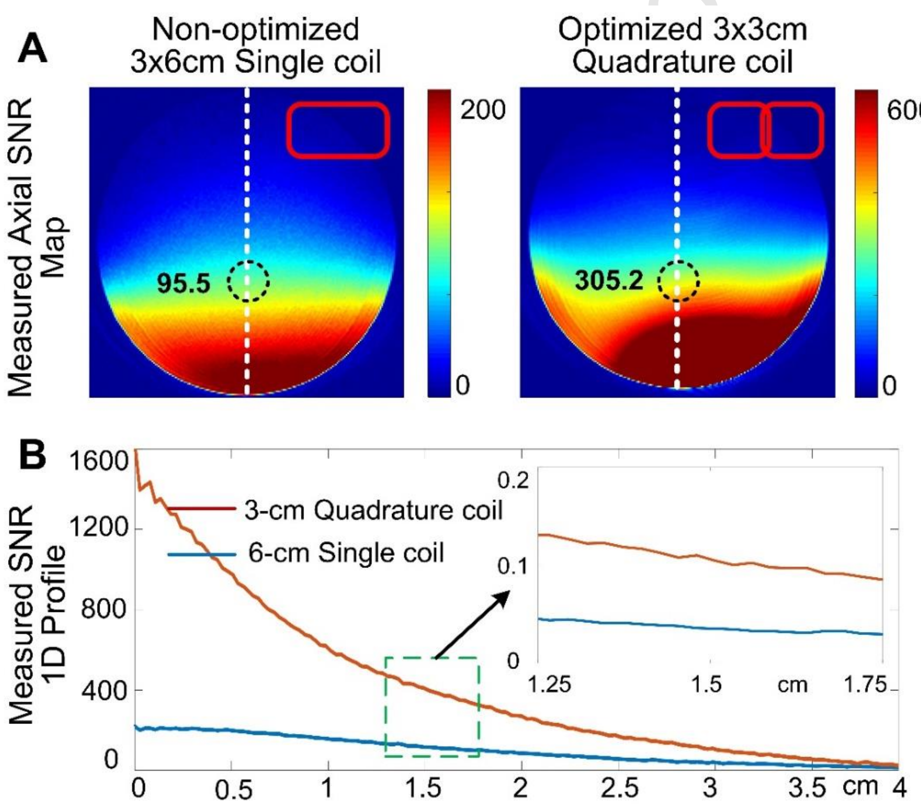

Figure 5 GRE images and measured axial SNR maps on a squirrel monkey using a non-optimized 6-cm-wide coil (top row) and an optimized 3-cm-width quadrature coil (bottom row). Similar to the SNR results on phantom, the optimized coil exhibits significant SNR improvement (up to 3.9 times) in the spinal cord area compared to the non-optimized coil. D: dorsal; V, ventral; R: rostral; C: caudal; Les, lesion; Ctrl: control. The transverse slice for the segment above the lesion was selected for SNR comparison. Images from a subject 4 months after unilateral dorsal column lesion were shown.

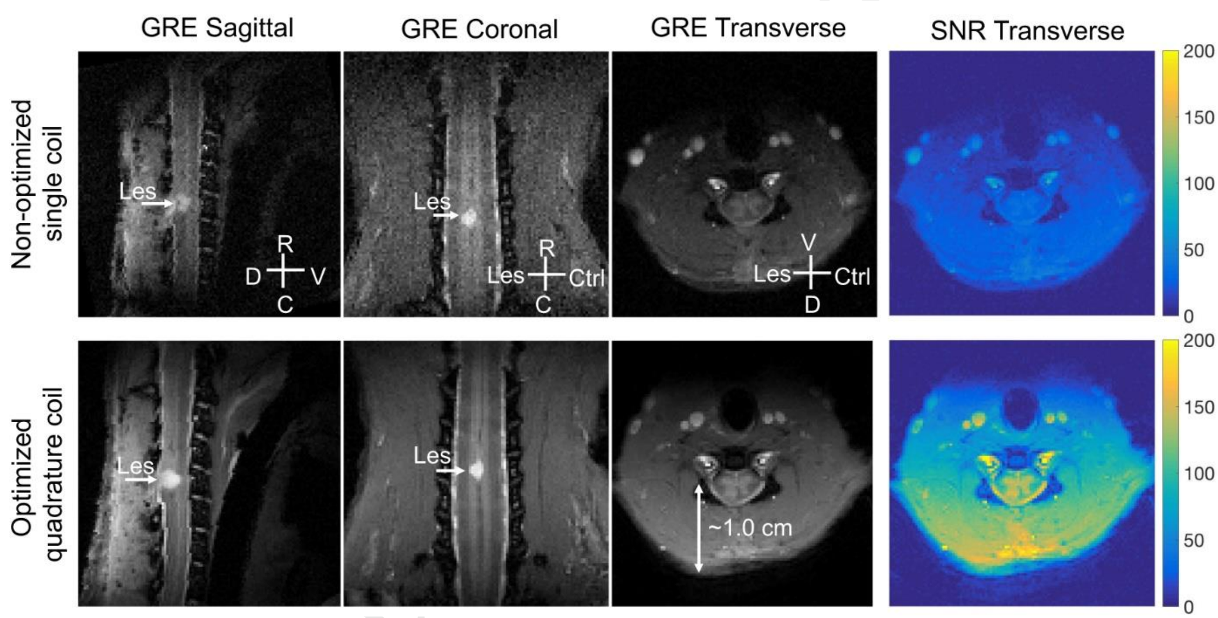

Manuscript title: Optimization of a transmit/receive surface coil for squirrel monkey spinal cord imaging

Author Contributions:

ML performed the electromagnetic simulation, fabricated the coil and analyzed the data, with help from XY. FW and LMC collected data on both phantom and the live squirrel monkey. XY and JCG conceived the idea and supervised the project. XY wrote the paper with input from all authors.